AGU PUBLICATIONS

Geophysical Research Letters

RESEARCH LETTER
10.1002/2016GL068895

Key Points:
- The presence of a partially molten magma body under a recently active volcano in Northeastern China
- Importance of using a dense enough local seismic array for such a study and not rely on distant seismic stations, as in previous studies
- Application of this technique for finding new energy resources such as potential sites for future geothermal exploitation

Supporting Information:
- Supporting Information S1

Correspondence to:
Z. Li,
zwli@whigg.ac.cn

Citation:
Li, Z., S. Ni, B. Zhang, F. Bao, S. Zhang, Y. Deng, and D. A. Yuen (2016), Shallow magma chamber under the Wudalianchi Volcanic Field unveiled by seismic imaging with dense array, *Geophys. Res. Lett.*, *43*, doi:10.1002/2016GL068895.

Received 22 FEB 2016
Accepted 20 APR 2016
Accepted article online 21 APR 2016

Shallow magma chamber under the Wudalianchi Volcanic Field unveiled by seismic imaging with dense array

Zhiwei Li[1], Sidao Ni[1], Baolong Zhang[1], Feng Bao[1], Senqi Zhang[2], Yang Deng[3], and David A. Yuen[4,5]

[1]State Key Laboratory of Geodesy and Earth's Dynamics, Institute of Geodesy and Geophysics, Chinese Academy of Sciences, Wuhan, China, [2]Center for hydrogeology and environmental geology survey, China Geological Survey, Baoding, China, [3]Earthquake Administration of Heilongjiang Province, Harbin, China, [4]School of Environment Sciences, China University of Geosciences, Wuhan, China, [5]Department of Earth Sciences, University of Minnesota, Twin Cities, Minneapolis, Minnesota, USA

Abstract The Wudalianchi Volcano Field (WDF) is a typical intraplate volcano in northeast China with generation mechanism not yet well understood. As its last eruption was around 300 years ago, the present risk for volcano eruption is of particular public interest. We have carried out a high-resolution ambient noise tomography to investigate the location of magma chambers beneath the volcanic cones with a dense seismic array of 43 seismometers and ~6 km spatial interval. Significant low-velocity anomalies up to 10% are found at 7–13 km depth under the Weishan volcano, consistent with the pronounced high electrical-conductivity anomalies from previous magnetotelluric survey. We propose these extremely low velocity anomalies can be interpreted as partial melting in a shallow magma chamber with volume at least 200 km^3 which may be responsible for most of the recent volcanic eruptions in WDF. Therefore, this magma chamber may pose a serious hazard for northeast China.

1. Introduction

We need a reliable knowledge of the distribution of magmatic chambers under volcanoes in order to evaluate the risk from powerful volcanic eruptions [*Jaxybulatov et al.*, 2014]. Three-dimensional velocity structures from seismic studies are sensitive to the volume of partial melting of the magma, which can produce significant low-velocity anomaly and provide important information on the distribution of possible magma chambers in the crust and upper mantle [*Husen et al.*, 2004; *Smith et al.*, 2009; *Masterlark et al.*, 2010; *Nagaoka et al.*, 2012; *Schmandt et al.*, 2012; *Farrell et al.*, 2014; *Jaxybulatov et al.*, 2014; *Seats and Lawrence*, 2014; *Huang et al.*, 2015]. Most previous studies were conducted to investigate the subsurface velocity structures beneath the volcanoes and successfully revealed the characteristics of magma chambers. With body wave traveltime tomographic methods, *Husen et al.* [2004], *Farrell et al.* [2014], and *Huang et al.* [2015] obtained the three-dimensional *P* and *S* wave velocity structures beneath the Yellowstone volcano field and depicted the spatial distribution of magma chamber characterized as prominent low-velocity anomalies.

Substantial advances in seismology have been made by the rapid progress in ambient noise tomography over the past decade [*Shapiro et al.*, 2005; *Yao et al.*, 2006; *Bensen et al.*, 2007; *Yang et al.*, 2007, 2011; *Lin et al.*, 2013], which leads to detailed upper crustal structures with dense seismic array in regions even without active earthquakes. The ambient noise tomography method has also been proven very effective in imaging magma distribution beneath the volcanoes [*Masterlark et al.*, 2010; *Nagaoka et al.*, 2012; *Seats and Lawrence*, 2014]. With the ambient noise surface wave tomography, *Seats and Lawrence* [2014], *Masterlark et al.* [2010] and *Nagaoka et al.* [2012] also found clear magma chambers underlying the Yellowstone Volcano Field, Okmok Volcano, and Mount Asama Volcano, respectively. Moreover, recent studies demonstrated conclusively that ambient noise tomography is a high-resolution method for probing shallow structures with a dense enough short-period seismic array [*Lin et al.*, 2013; *Fang et al.*, 2015]. This development has proved the feasibility for unveiling 3-D velocity anomalies with small scales of a few kilometers.

The Wudalianchi Volcano Field (WDF) is situated in Northeast China, about 1800 km away from the Pacific plate and 400 to 600 km from the Changbaishan and Jingbohu volcanoes (Figure 1). The volcanic activities in WDF are considered to be typically characteristic of intraplate volcanoes. Laboratory experiments on the peridotite xenoliths in WDF yielded information about the estimates melt equilibration temperatures of

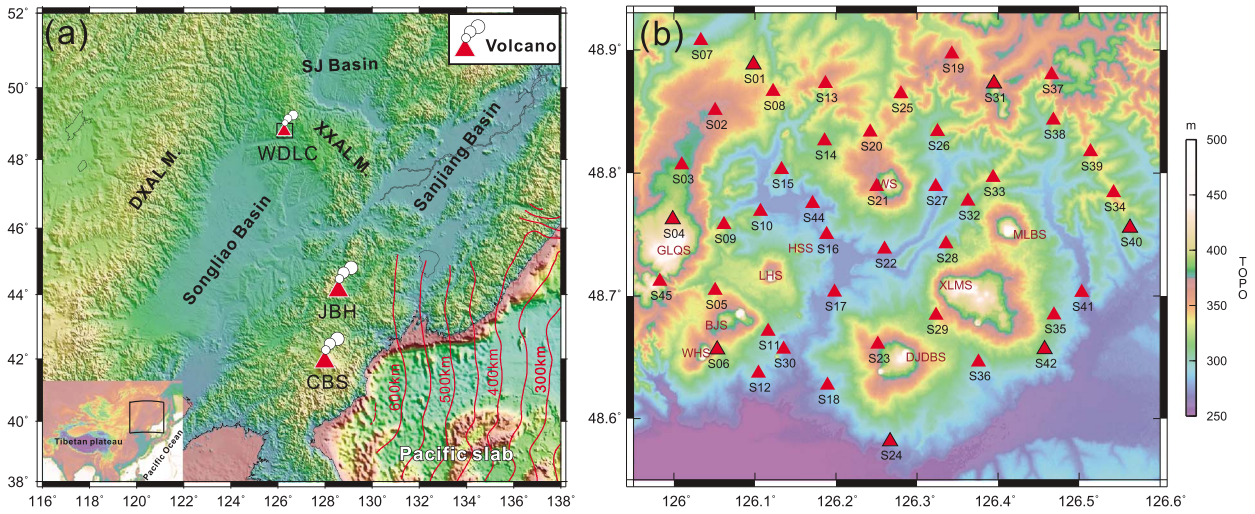

Figure 1. Location of the geographical area being studied and WDF. (a) Tectonic characteristics around the WDF (WDLC, Wudalianchi Volcano Field; JBH, Jingbohu Volcano; CBS, Changbaishan Volcano; DXAL M., Daxianganling Mountain; XXAL M., Xiaoxinganling Mountain; SJ Basin, Sunwu-Jiayin Basin). The black rectangular in the subfigure in the lower-right corner shows the region of Figure 1a. The black rectangular in the Figure 1a near the WDF shows the location of Figure 1b. (b) Distribution of temporary dense seismic array with topographical map. Red triangles indicate the locations of seismic stations (WS, Weishan Volcano; MLBS, Molabu Volcano; XLMS, Xilongmenshan Volcano; DJDBS, Dongjiaodebushan Volcano; WHS, Wohushan Volcano; BJS, Bijiashan Volcano; LHS, Laoheishan Volcano; HSS, Huoshaoshan Volcano; GLQS, Gelaqiushan Volcano).

959–1127°C and pressures of 1.27–3.37 GPa, corresponding to mantle-derived magma from 80 to 100 km depth [*Shao and Zhang*, 2008]. The WDF is bounded by the Xiaoxinganling Mountain to the northeast, Daxinganling Mountain to the northwest, and Songliao Basin to the south and is tectonically controlled by the Cenozoic NNW strike intracontinental rift (Figure 1). The WDF consists of 14 Cenozoic monogenetic scoria cones and associated lavas with high-K basalt composition [*Shao et al*., 2008]. The Laoheishan volcano cone, Huoshaoshan volcano cone, and Weishan volcano cone are located in the center of the WDF (Figure 1). The volcanic activity of the WDF began in the early Pleistocene, reached its most active period in the middle Pleistocene, and became active again since Holocene [*Xia*, 1990; *Shao et al*., 2008]. The most recent eruption of the WDF occurred around 300 years ago at the Laoheishan and Huoshaoshan volcano cones, and the explosive of scoria cone formation and effused lava extended to a area of ~ 68 km^2 [*Xia*, 1990; *Shao et al*., 2008]. Considering the relatively short history since its most recent eruption, we may expect the magmatic system responsible for the volcanic eruption to be still present in a partial melting status from the middle to upper crusts near the volcanic cones. Therefore, we recognize the WDF to be a potentially good site for exploring the possible cooling magmatic system beneath active volcanoes. Previous geological and geophysical studies proposed potential magma chambers at 3–20 km depth [*Xia*, 1990; *Shao et al*., 2008; *Zhan et al*., 2006; *Zhang et al*., 2015]. Teleseismic traveltime tomography [*Zhang et al*., 2014], receiver functions studies [*He et al*., 2003; *Zhang et al*., 2013], and *Pn* wave attenuation tomography [*Zhao et al*., 2015] also revealed low-velocity anomalies in the lower crust and upper mantle, strong attenuation in the uppermost mantle and complex Moho discontinuities in the WDF, suggesting that the mantle-derived basaltic melt may further fuel the crustal magma chamber.

Previous studies in WDF were limited by very sparse network of seismic stations (only at most a couple of permanent stations), thus suffering from very low resolution of 50 to 100 km which is not sufficient for detailed velocity anomalies beneath the volcano cones in WDF. In this study we have deployed a dense temporary seismic array with 43 seismometers to resolve reliably small-scale anomalies, which may yield clues about magma chambers.

2. Data and Method

These seismometers have a frequency band of 0.2–100 Hz with a natural frequency of 4.5 Hz. These three-component seismometers were deployed in the WDF with an interval of ~6 km for ~35 days during September and October 2014 (Figure 1). GPS was used for timing inside the seismic data acquisition system. This dense seismic array can cover most volcano cones in WDF. The Weishan volcano cone is located nearly in

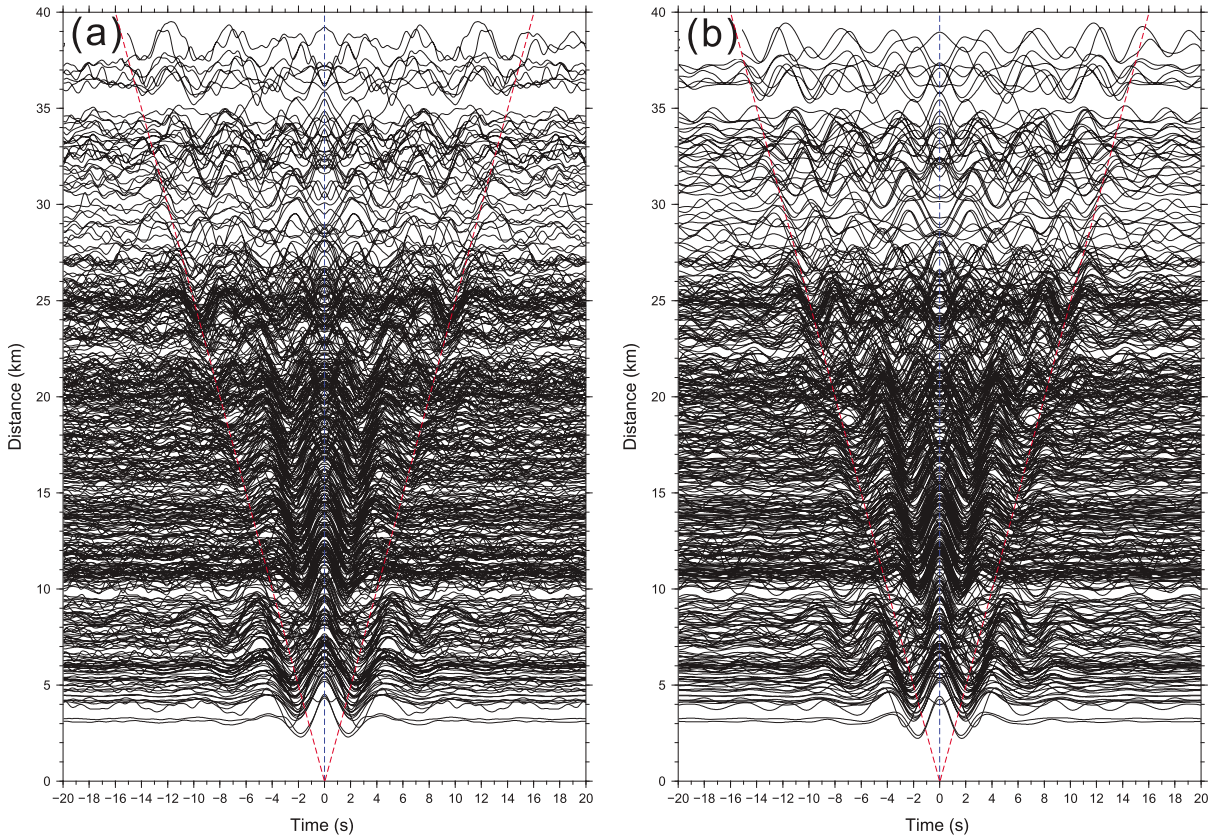

Figure 2. Noise cross-correlation functions (NCFs) extracted from the ambient noise seismic waveforms. The red dashed lines show the reference velocity of 2.5 km/s. (a) NCFs with 0.1–1 Hz band-pass filter; (b) NCFs with 0.2–0.5 Hz band-pass filter.

the center of the seismic array (Figure 1b), which can yield adequate tomographic resolution beneath the Weishan volcano cone. Ambient noise waveforms on the vertical component are used to extract Rayleigh waves at 0.8–8 s period from the noise cross-correlation functions carried out over a 5 week period. Due to the strong scattering and attenuation, surface waves at this high frequency are difficult to extract for interstation distances of hundreds of kilometers [*Yao et al*., 2006; *Yang et al*., 2007, 2011]. However, we still can detect high-frequency (0.5–4 Hz) Rayleigh waves at small interstation distance within several thousand meters for dense seismic array, which has been proven effective for imaging shallow 3-D shear wave velocity structures [*Lin et al*., 2013; *Fang et al*., 2015].

We follow the modified method proposed by *Bensen et al*. [2007] to conduct the waveform cross-correlation calculations. Continuous waveforms are cut into 1 h segment, then demeaned, and detrended. Spectrum whitening and normalization of the waveform are also applied on each waveform segment. All noise cross-correlation functions for each station pair are stacked and averaged by the positive and negative lags to improve the signal-to-noise ratio. Clear Rayleigh waves are observed in the noise cross-correlation functions after 0.1–1 Hz and 0.2–0.5 Hz band-pass filter (Figure 2). Cross-correlation functions of similar distance are stacked with different band-pass filters to render a clearer Rayleigh waveform (Figure S1 in the supporting information). Multiple filter waveforms for station pairs with 9–36 km interstation distance are also shown in Figure S2. The signal-to-noise ratio varies with the interstation distance and the frequency band for band-pass filter. Surface wave shows higher signal-to-noise ratio at lower frequencies at longer interstation distance (Figure S2). Multiple filter technique is applied to the noise cross-correlation functions to obtain the dispersion curve of the Rayleigh group velocity between 0.8 and 8 s [*Herrmann*, 2013]. Group velocity dispersions with interstation distance less than 1.5 wavelength are rejected. After data quality control, totally 260 dispersion curves from cross-correlation functions with signal-to-noise ratio $>$ 3.5 are obtained from 903 station pairs. With these dispersion data, we then carry out inversion of Rayleigh wave group velocity at 0.8–8 s periods by an iterative nonlinear tomographic method with a fast marching method

(FMM) using a subspace inversion algorithm [*Sethian*, 1996; *Rawlinson and Sambridge*, 2004]. Since great-circle assumption of surface wave propagation no longer holds in a strongly lateral heterogeneous media [*Woodhouse*, 1974; *Dahlen and Tromp*, 1998] especially at the shallow crustal depth, the FMM can account for raypath bending off great circle and could improve the tomographic results. The 3-D shear wave velocity inversion is conducted with linear inversion method based on the tomographic group velocity maps at different periods [*Herrmann*, 2013]. We analyzed the depth sensitivity kernels for 1–8 s Rayleigh wave group velocity dispersions on the shear wave velocity. Although the most sensitivity depth of 6–8 s period waves is at 4–8 km depth, the dispersions still have sensitivity to the structures up to 10–13 km (Figure S3). Therefore, the shear wave velocity structure deep to 13 km is included in the inversion. But we should bear in mind that the deeper structures are less reliably resolved.

3. Results

In order to evaluate the resolution of the group velocity tomographic results, we have performed checkerboard resolution tests. Based on the resolution tests, we can show that most areas are well resolved except at the margin of the seismic array (Figures S4 and S5). Moreover, better resolutions are obtained at 1.4–5 s periods than those at longer periods of 6–8 s. This result can be attributed to the relative sparse raypath coverage at longer periods. The resolution near the Weishan volcano cone is generally adequate at all periods because it is nearly located in the center of the seismic array. In addition to the checkerboard resolution test, we also conducted the uncertainty estimation for the shear wave velocity structures by the bootstrap method [*Koch*, 1992; *Hearn and Ni*, 1994]. The Rayleigh wave traveltimes at each period are randomly selected from the observed data set to construct the data set for tomographic inversion. We then carry out shear wave velocity inversion at each grid with the dispersion curve. We keep the inversion parameters (e.g., damping, smoothness, and grid spacing) the same in the bootstrap test, as in the inversion with real data. With 200 shear wave velocity models from the bootstrap inversions, we calculate standard deviations for the velocity structures at all depths (Figure S6). For most depths, the standard deviations are less than 0.15 km/s; for deeper depth of 11–13 km, the maximum standard deviation increases to 0.20 km/s. However, the standard deviations are generally much less than the imaged significant velocity anomalies (0.3–0.8 km/s) (Figure 3). Therefore, uncertainties will not bias the analysis on the magma chamber with strong velocity contrast, especially in areas near the center of the dense seismic array. Results show that adequate resolution down to ~ 13 km depth is achieved for areas covered with this dense seismic array. Velocity changes at the margin of the dense seismic array or at depths deeper than 13 km are not able to be resolved adequately. Figure S7 shows a good fitting of dispersion curves before and after shear wave velocity inversion at five locations, thus demonstrating a good enough quality for the ambient noise tomography.

Horizontal slices of shear wave velocity structures at 1–13 km are displayed in Figure 3. In general, we can see strong lateral variations of shear wave velocities in the WDF. At 1–5 km depth, significant low-velocity anomalies with amplitude of −10% appear in the areas between the Weishan and Laoheishan volcano cones. For greater depth of 7–13 km, strong low-velocity anomalies become more conspicuous beneath the Weishan volcano cone, contrasting to the normal to relatively high velocity anomalies in surrounding areas. The cross sections through the Weishan volcano cone show sharper velocity contrasts (Figure 4). Low-velocity bodies beneath the Weishan volcano cones are mostly found at depths shallower than ~4 km or deeper than ~7 km, and the width of the anomaly below 7 km depth is about 6–8 km. Whereas at a depth of 4–7 km the velocity anomaly remains lower than its surrounding material at the same depth (Figure 4a). Likewise, strong low-velocity characteristics are also found at 0–4 km and 7–13 km depth beneath the Molabu volcano cone, and a weak, thin low-velocity belt beneath the Xilongmenshan volcano cone from the surface down to ~13 km depth (Figure 4c). In addition in Figure 4c, compared to the velocity anomaly beneath the Weishan and Molabu volcano cones, different characteristics are found beneath the Laoheishan and Huoshaoshan volcano cones. As shown previously in Figure 4b, strong low-velocity anomalies extend deep to ~ 7 km from the surface beneath the Laoheishan volcano cone, which is much deeper than the ~ 3 km depth of the low-velocity body beneath the Huoshaoshan volcano cone.

4. Discussions

Since the most recent volcanic eruption in WDF occurred, the magmatic system could still retain partial melting with high temperature in the middle to upper crust near the volcanic cones. With geochemical

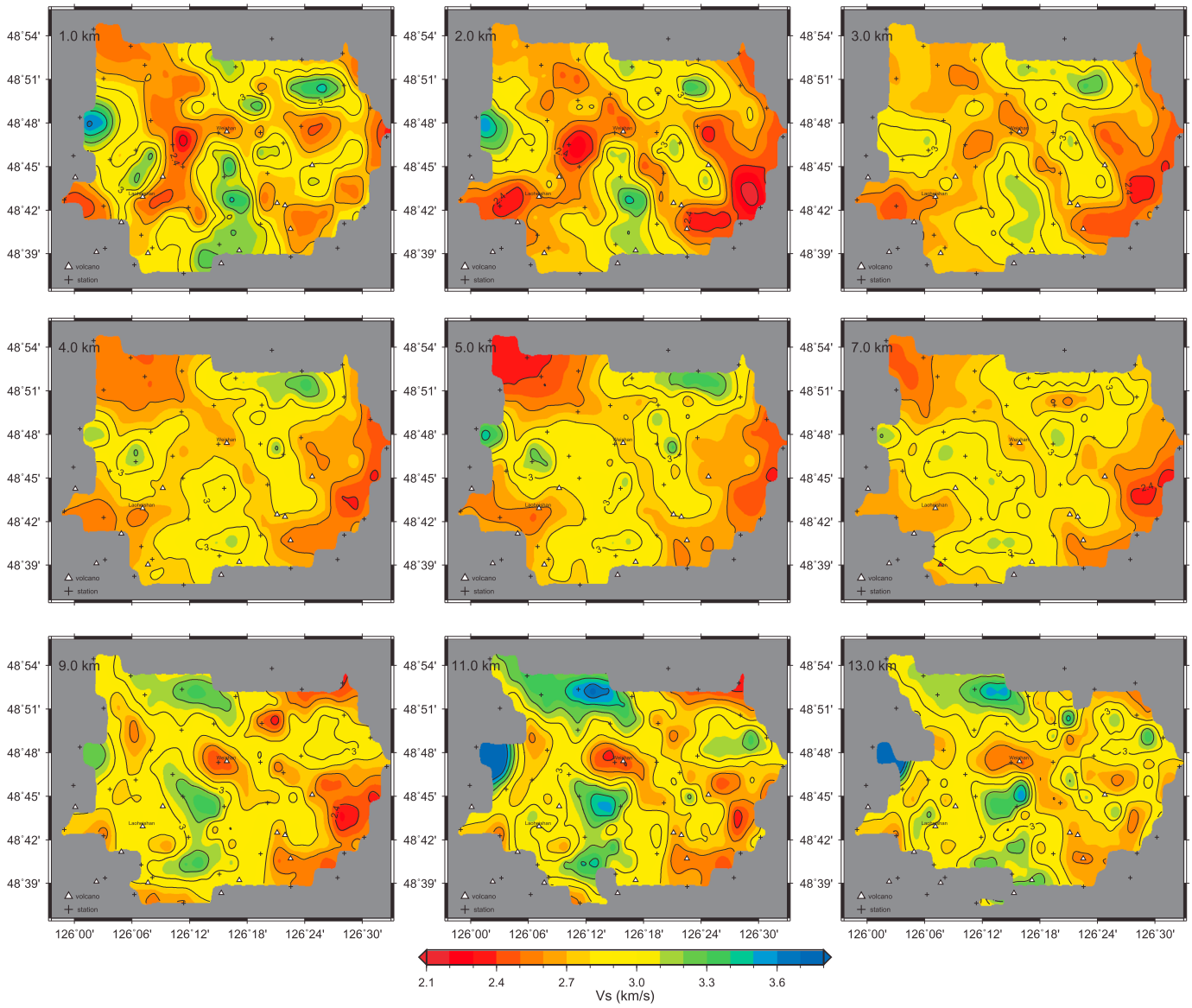

Figure 3. Tomographic images for shear wave velocities at depths from 1 to 13 km. The depth for each subfigure is labeled on the upper-left corner. The areas with few data coverage are masked by gray color approximately according to the raypath distribution at different periods of dispersive surface waves. The crosses indicate the locations of the temporary seismic stations. Red triangles show the locations of volcano cones in the WDF.

constraints based on the crystallization pressure of olivine in the lava flow, *Xia* [1990] inferred that the depth for the quaternary magma chamber cannot be shallower than 3–4 km depth. The latest magnetotelluric (MT) survey [*Zhang et al*., 2015] around the Weishan volcano cone also found significant high electric conductivity anomaly at 5–9 km depth (for depths deeper than 9 km, no good resolution obtained for this MT survey), and relatively low to normal electric conductivity anomalies at shallower depth. Different characteristics of the velocity and electric conductivity structures may suggest distinct interpretations for the two low-velocity anomalies shallower than 4 km and deeper than 7 km beneath the Weishan volcano cone. The low-velocity anomalies at shallower depth (<4 km) here may represent an area with highly fractured fluid-filled volume rather than an area filled with magmatic fluids (gas, hydrothermal fluids, and melt) migrated to shallower depths away from the magma chamber at deeper depth (e.g., the Hot Spring Basin Group in the Yellowstone volcanic field) [*Farrell et al*., 2014]. In the Yellowstone volcanic filed, the shallow (0–3 km) low-velocity body beneath the Hot Spring Basin Group clearly connects to the proposed main body of magma chamber down to 5–14 km beneath the Yellowstone Caldera, which supports the magmatic fluids migrating

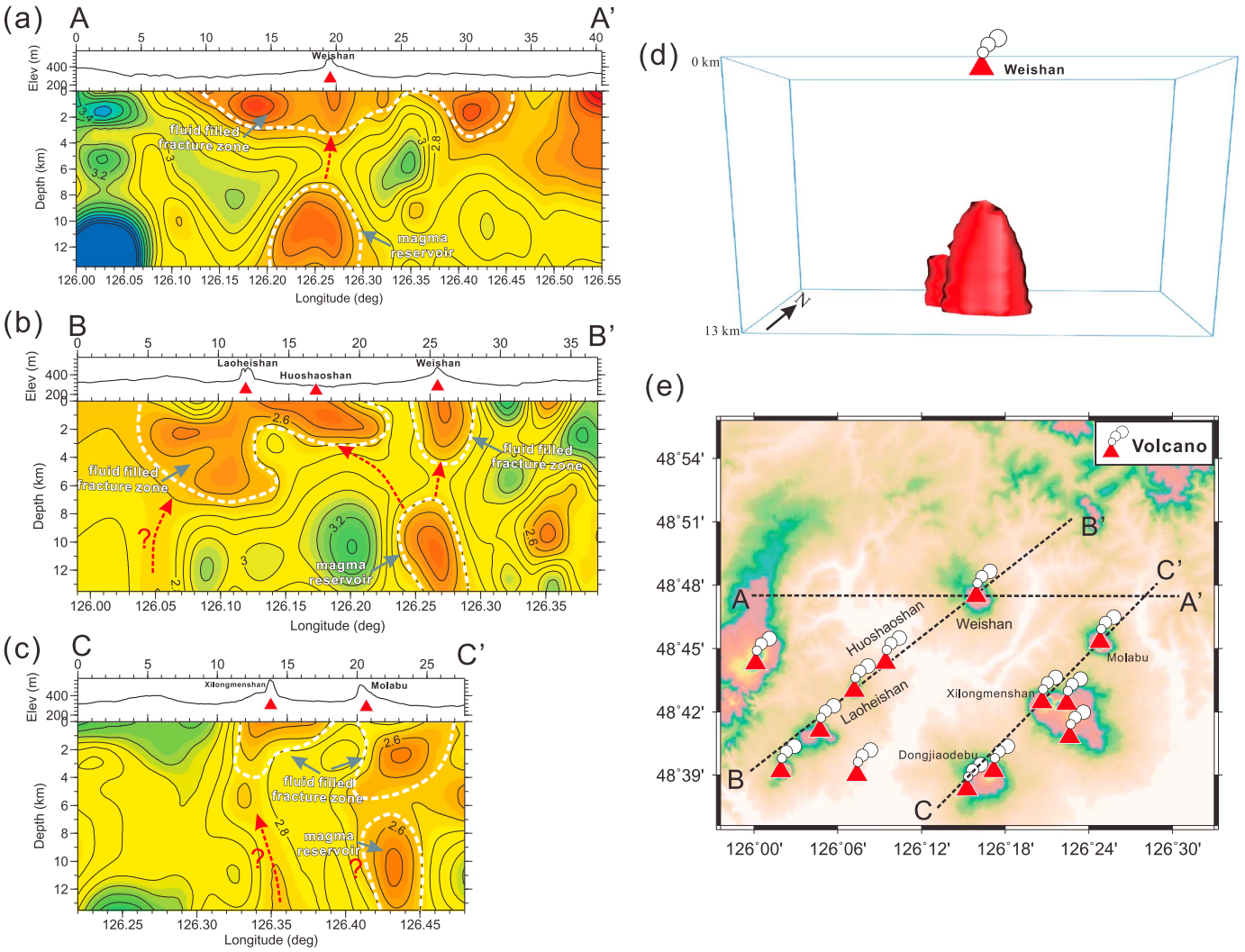

Figure 4. (a–c) Cross sections of shear wave velocity crossing Weishan, Laoheishan, Huoshaoshan, Molabu, and Xilongmenshan volcanos. Red triangles indicate the volcano cones along the cross sections. (d) The −10% shear wave velocity isosurface of the magma chamber beneath the Weishan volcano cone. (e) Location map of the cross sections.

to shallower depth [*Farrell et al.*, 2014; *Huang et al.*, 2015]. While in the WDF, the low-velocity anomalies at shallower (≲4 km) or deeper (≳7 km) depths beneath the Weishan and Molabu volcano cones can be observed to be separated into two bodies (Figures 4a–4c). In addition, there are no apparent hydrothermal alterations around the Weishan and Molabu volcano cones, or around the Laoheishan and Huoshaoshan volcano cones. Therefore, we infer that the low-velocity anomalies at shallower depth (≲4 km) beneath the Weishan, Molabu, and Xilongmenshan volcano cones, as well as the shallow low-velocity bodies ≲7 km beneath the Laoheishan volcano cone and ≲3 km beneath the Huoshaoshan volcano cone (Figures 4a–4c), can be attributed to the highly fractured fluid-filled volumes (e.g., meteoric or surface-derived water circulating in the fractures) rather than magma chambers [*Farrell et al.*, 2014; *Diaz et al.*, 2015].

As for the low-velocity body at 7–13 km depth beneath the Weishan volcano cone (see Figures 4a and 4b), we can infer that it is a magma chamber with magmatic fluids and partial melt at high temperature. These characteristics are also consistent with the high electric conductivity anomaly shown at 5–9 km depth in the MT survey by *Zhang et al.* [2015]. Similar low-velocity anomalies at 5–15 km depth are also found and interpreted as magma chambers beneath the active Mount Asama volcano in Japan [*Nagaoka et al.*, 2012], Yellowstone Caldera [*Husen et al.*, 2004; *Farrell et al.*, 2014; *Seats and Lawrence*, 2014; *Huang et al.*, 2015], Toba Volcano,

Indonesia [*Jaxybulatov et al*., 2014], and the Lastarria volcano in Chile [*Diaz et al*., 2015]. The negative 10% shear wave velocity isosurface under the Weishan volcano cone is also shown in Figure 4d, and only low velocity materials deeper than 6 km are not included. Similarly, the low-velocity body at deeper depth than ~ 7 km beneath the Molabu volcano cone may also suggest a magma chamber with magmatic fluids and partial melt at high temperature. Moreover, for the thin mildly low velocity belt beneath the Xilongmenshan volcano cone, it is also tempting to interpret it as a magma conduit connected to the magma chamber in the deeper depth. However, due to the relatively lower resolution and the absence of the MT surveys in this area, further geophysical surveys (e.g., a dense seismic array, MT) are needed to improve the resolution and confirm the low-velocity anomalies.

Based on the resolution of our tomographic results, we estimate that the magma chamber may have volume at least 200 km^3 (~$6 \times 6 \times 6$ km) underneath the Weishan volcano, which is a factor of ~50 smaller than the upper crustal magma chamber or a factor of ~200 smaller than the lower crustal magma chamber underneath the Yellowstone [*Farrell et al*., 2014; *Huang et al*., 2015]. However, it is comparable to the magma chambers underneath the Mount Asama volcano in Japan [*Nagaoka et al*., 2012] and the Okmok Volcano in Alaska [*Masterlark et al*., 2010]. The magma chamber may be not the only one beneath the WDF due to that totally 14 volcano calderas located in a ~ 40×40 km area. Based on our tomographic results, we can conjecture that the magma chamber beneath the Weishan volcano cone can connect the volcanic conduit from the lower crust to the volcanic calderas of the Weishan, Laoheishan, Huoshaoshan, Molabu, and Xilongmenshan volcanoes and may be responsible for the most recent volcanic eruptions. If this can be proved to be correct, then we can further argue that although the upward magmatic migration from this magma chamber is temporarily closed by high-velocity materials at 4–7 km beneath the Weishan volcano cone, this can seriously impact the physics of magma recharge and migration, as well as the volcanic eruption risk, due to that the magma conduit connected to the lower crust still exists today.

Because the tomography is limited by the wavelength of the short-period ($<$8 s) Rayleigh wave, we cannot resolve the magma chamber distribution at greater depth ($>$13 km) based on these tomographic results. Previous geophysical studies still can provide some information on the structures in the middle-lower crust and upper mantle. *Zhan et al*. [2006] conducted a MT survey near the Laoheishan and Huoshaoshan volcano cones, and they found a rivet-shaped high electric conductivity anomaly body down to a depth of 20 km from southwest to northeast, which can be interpreted as a partial-melting body. Seismic studies with teleseismic receiver functions [*He et al*., 2003; *Zhang et al*., 2013], teleseismic *S* wave traveltime tomography [*Zhang et al*., 2014], and *Pn* wave attenuation tomography [*Zhao et al*., 2015] have also revealed low-velocity anomalies in the lower crust and upper mantle, strong attenuation in the uppermost mantle, and complex Moho discontinuities beneath the WDF. Both geochemical and petrological studies have also suggested that the magma source in the WDF comes from the mantle [*Shao et al*., 2008; *Shao and Zhang*, 2008]. These results may suggest that the basaltic melt can rises buoyantly from the upper mantle to the Moho and then to lower crust and fuels the magma chamber in the middle-upper crust with partially melting silicic continental crust.

5. Conclusions

Seismic imaging with a dense seismic array can provide new insights on the magma chamber distribution and volcanic eruption risk in the WDF. With the temporally installed local array, we have obtained the best resolution in the WDF up to now, and substantially improved understanding of the magmatic system than previous studies. This makes it possible to delineate small size crustal magma chamber with a scale of a few kilometers. A potential magma chamber is revealed by this study to be at 7–13 km depth beneath the Weishan volcano cone, which may have a volume of at least 200 km^3. Magma distributions at deeper depth also possibly exist based on previous seismic and MT studies [*Zhan et al*., 2006; *He et al*., 2003; *Zhang et al*., 2013; *Zhao et al*., 2015], where the basaltic melt buoyantly rises from the upper mantle through the Moho and lower crust and fuels the magma chamber in shallow crust with partially melting materials. However, the crustal magma chamber founded by this study could be one of several magma chambers beneath the WDF, which only fuels the volcanic eruptions for Laoheishan, Huoshaoshan, and Weishan volcanoes. In addition, since small-scale volcanic magma conduits still possibly exist in middle-lower crust and upper mantle, the upward magmatic migration from deeper depth may recharge the magma chamber. Therefore, the WDF still bear on the eruptive potential, at least close by the Laoheishan, Huoshaoshan, and Weishan

volcanoes, possibly near the Molabu and Xilongmenshan volcanoes. Although seismic imaging in this study provides detailed information on the magma system in the WDF, reliable resolutions are found only at depth shallower than ~13 km and only in the central areas of the WDF (Figures S4 and S5). Therefore, we need to pursue further with both seismic observations at longer length and time scales to delineate more clearly the entire magmatic system on the middle-lower crust and upper mantle in order to analyze its relationship to the magma chamber in the shallow crust. This work suggests the possible presence of partially molten magma in shallow crust under WDF. The tools and method developed here also are helpful for geothermal exploration in northeast China and then elsewhere in the world.

Acknowledgments

Data employed in this study were from the archives of State Key Laboratory of Geodesy and Earth's Dynamics, Institute of Geodesy and Geophysics, Chinese Academy of Sciences, which operates and archives data from the dense seismic array in Wudalianchi Volcanic Filed. The seismic data eventually will be publicly accessible. We thank Li Zhao and Huajian Yao for their helpful comments on this study. This study is supported by China Geological Survey (12120114025001), XDB06030203, NSFC41304045, and 2014CB845903, 2013CB733204, XH15014Y, and Youth Innovation Promotion Association CAS. We appreciate the constructive and critical reviews by the Editor, Jeroen Ritsema, and two anonymous reviewers.

References

Bensen, G. D., M. H. Ritzwoller, M. P. Barmin, A. L. Levshin, F. Lin, M. P. Moschetti, N. M. Shapiro, and Y. Yang (2007), Processing seismic ambient noise data to obtain reliable broad- and surface wave dispersion measurements, *Geophys. J. Int.*, *169*, 1239–1260.

Dahlen, F. A., and J. Tromp (1998), *Theoretical Global Seismology*, Princeton Univ. Press, N. J.

Diaz, D., W. Heise, and F. Zamudio (2015), Three-dimensional resistivity image of the magmatic system beneath Lastarria volcano and evidence for magmatic intrusion in the back arc (Northern Chile), *Geophys. Res. Lett.*, *42*, 5212–5218, doi:10.1002/2015GL064426.

Fang, H. J., H. J. Yao, H. J. Zhang, Y.-C. Huang, and R. D. van der Hilst (2015), Direct inversion of surface wave dispersion for three-dimensional shallow crustal structure based on ray tracing: methodology and application, *Geophys. J. Int.*, *201*, 1251–1263.

Farrell, J., R. B. Smith, S. Husen, and T. Diehl (2014), Tomography from 26 years of seismicity revealing that the spatial extent of the Yellowstone crustal magma reservoir extends well beyond the Yellowstone caldera, *Geophys. Res. Lett.*, *41*, 3068–3073, doi:10.1002/2014GL059588.

He, C. S., C. Y. Wang, and J. P. Wu (2003), The velocity structure of crust and upper mantle in the Wudalianchi Volcano area inferred from the receiver function, *Chinese J. Geophys.*, *25*(2), 128–135.

Hearn, M., and J. F. Ni (1994), *Pn* velocities beneath continental collision zones: The Turkish-Iranian Plateau, *Geophys. J. Int.*, *117*, 273–283.

Herrmann, R. B. (2013), Computer programs in seismology: An evolving tool for instruction and research, *Seismol. Res. Lett.*, *84*, 1081–1088.

Huang, H. H., F. C. Lin, B. Schmandt, J. Farrell, R. B. Smith, and V. C. Tsai (2015), The Yellowstone magmatic system from the mantle plume to the upper crust, *Science*, *348*, 773–776.

Husen, S., R. B. Smith, and G. P. Waite (2004), Evidence for gas and magmatic sources beneath the Yellowstone volcanic field from seismic tomographic imaging, *J. Volcanol. Geotherm. Res.*, *131*(3), 397–410.

Jaxybulatov, K., N. M. Shapiro, I. Koulakov, A. Mordret, M. Landès, and C. Sens-Schönfelder (2014), A large magmatic sill complex beneath the Toba caldera, *Science*, *346*, 617–619.

Koch, M. (1992), Bootstrap inversion for vertical and lateral variations of the S wave structure and the V_p/V_s-ratio from shallow earthquakes in the Rhinegraben seismic zone, Germany, *Tectonophysics*, *210*, 91–115.

Lin, F. C., D. Li, R. W. Clayton, and D. Hollis (2013), High-resolution 3D shallow crustal structure in long beach, California: Application of ambient noise tomography on a dense seismic array, *Geophysics*, *78*(4), Q45–Q56.

Masterlark, T., M. Haney, H. Dickinson, T. Fournier, and C. Searcy (2010), Rheologic and structural controls on the deformation of Okmok volcano, Alaska: FEMs, InSAR, and ambient noise tomography, *J. Geophys. Res.*, *115*, B02409, doi:10.1029/2009JB006324.

Nagaoka, Y., K. Nishida, Y. Aoki, M. Takeo, and T. Ohminato (2012), Seismic imaging of magma chamber beneath an active volcano, Earth planet, *Sci. Lett.*, *333*, 1–8.

Rawlinson, N., and M. Sambridge (2004), Waveform evolution in strongly heterogeneous layered media using the fast marching method, *Geophys. J. Int.*, *156*(3), 631–647.

Schmandt, B., K. G. Dueker, E. D. Humphreys, and S. H. Hansen (2012), Hot mantle upwelling across the 660 beneath Yellowstone, *Earth Planet. Sci. Lett.*, *331–332*, 224–236.

Seats, K. J., and J. F. Lawrence (2014), The seismic structure beneath the Yellowstone Volcano Filed from ambient seismic noise, *Geophys. Res. Lett.*, *41*, 8277–8282, doi:10.1002/2014GL061913.

Sethian, J. A. (1996), A fast marching level set method for monotonically advancing fronts, *Proc. Nat. Acad. Sci.*, *93*(4), 1591–1595.

Shao, J. A., and W. L. Zhang (2008), The evolving belt-Wudalianchi volcanic rock belt, *Earth Sci. Front.*, *15*(6), 241–250.

Shao, J. A., W. L. Zhang, and C. Zhang (2008), Mantle enrichment of Wudalianchi volcanic rock belt, *Acta Petrol. Sin.*, *24*(11), 2485–2494.

Shapiro, N. M., M. Campillo, L. Stehly, and M. H. Ritzwoller (2005), High-resolution surface wave tomography from ambient seismic noise, *Science*, *307*(5715), 1615–1618.

Smith, R. B., M. Jordan, B. Steinberger, C. M. Puskas, J. Farrell, G. P. Waite, S. Husen, W.-L. Chang, and R. O'Connell (2009), Geodynamics of the Yellowstone hotspot and mantle plume: Seismic and GPS imaging, kinematics, and mantle flow, *J. Volcanol. Geotherm. Res.*, *188*, 26–56.

Woodhouse, J. H. (1974), Surface waves in a laterally varying layered structure, *Geophys. J. R. Astron. Soc.*, *37*, 461–490.

Xia, L. Q. (1990), On the evolution of volcanic magma from Wudalianchi, China, *Acta Petrol. Sin.*, *1*, 13–27.

Yang, Y., M. H. Ritzwoller, and C. H. Jones (2011), Crustal structure determined from ambient noise tomography near the magmatic centers of the Coso region, southeastern California, *Geochem. Geophys. Geosyst.*, *12*, Q02009, doi:10.1029/2010GC003362.

Yang, Y., M. H. Ritzwoller, A. L. Levshin, and N. M. Shapiro (2007), Ambient noise Rayleigh wave tomography across Europe, *Geophys. J. Int.*, *168*, 259–274.

Yao, H. J., R. D. van der Hilst, and M. V. de Hoop (2006), Surface-wave array tomography in SE Tibet from ambient seismic noise and two-station analysis. I: Phase velocity maps, *Geophy. J. Int.*, *166*, 732–744.

Zhang, S. Q., Z. W. Li, P. Y. Tian, et al. (2015), Integrated study on the geological and geophysical survey in the Wudalainchi Volcano Field, China Geol. Surv. Rep., 1–110, Baoding.

Zhang, G. C., Q. J. Wu, J. T. Pan, F. X. Zhang, and D. X. Yu (2013), Study of crustal structure and Poisson ration of NE China by H-K stack and CCP stack methods, *Chin. J. Geophys.*, *56*(12), 4084–4094.

Zhang, F. X., Q. J. Wu, and Y. H. Li (2014), A traveltime tomography study by teleseismic *S* wave data in the Northeast China area, *Chin. J. Geophys*, *57*(1), 88–101.

Zhan, Y., G. Z. Zhao, J. J. Wang, Q. B. Xiao, J. Tang, and I. I. Rokityansky (2006), Crustal electric conductivity structure for Wudalianchi volcanic cluster in the Heilongjiang Province, China, *Acta Petrol. Sin.*, *22*(6), 1494–1502.

Zhao, L. F., X. B. Xie, B. F. Tian, Q. F. Chen, T. Y. Hao, and Z. X. Yao (2015), *Pn* wave geometrical spreading and attenuation in Northeast China and the Korean Peninsula constrained by observations from North Korean nuclear explosions, *J. Geophys. Res. Solid Earth*, *120*, 7558–7571, doi:10.1002/2015JB012205.

Geophysical Research Letters

Supporting Information for

Shallow Magma Chamber under the Wudalianchi Volcanic Field Unveiled by Seismic Imaging with Dense Array

Zhiwei Li[1], Sidao Ni[1], Baolong Zhang[1], Feng Bao[1], Senqi Zhang[2], Yang Deng[3], David Yuen[4,5]

[1]State Key Laboratory of Geodesy and Earth's Dynamics, Institute of Geodesy and Geophysics, Chinese Academy of Sciences, Wuhan 430077, China, [2]Center for hydrogeology and environmental geology survey, China Geological Survery, Baoding 071051, China, [3]Seismological Bureau of Heilongjiang Province, China Earthquake Administration, Harbin 150090, China, [4]School of Environment Sciences, China University of Geosciences, 430074 Wuhan, China, [5] Department of Earth Sciences, University of Minnesota, Minneapolis, MN 55455, USA

Contents of this file

Figures S1 to S7

Introduction

This supporting information provides the supplementary figures for the main article.

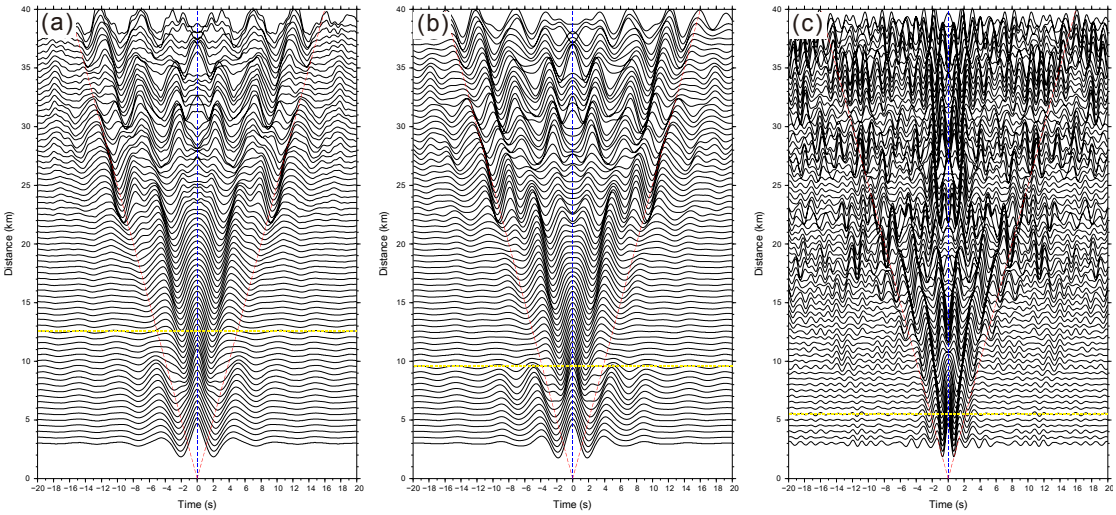

Figure S1. Noise cross-correlation functions (NCFs) extracted from the ambient noise seismic waveforms. The NCFs are stacked within ±1.5 km intervals relative to the central distance. The red dashed line shows the reference velocity of 2.5 km/s. (a) NCFs with 0.1~1.0 Hz band-pass filter; (b) NCFs with 0.2~0.5 Hz band-pass filter; (c) NCFs with 0.5~1.0 Hz band-pass filter. The Yellow dashed line shows the1.5 wavelength cutoff distance relative to velocity of 2.5 km/s. The reference frequencies are 0.3, 0.4 and 0.7 Hz for Figure S2a, S2b and S2c, respectively.

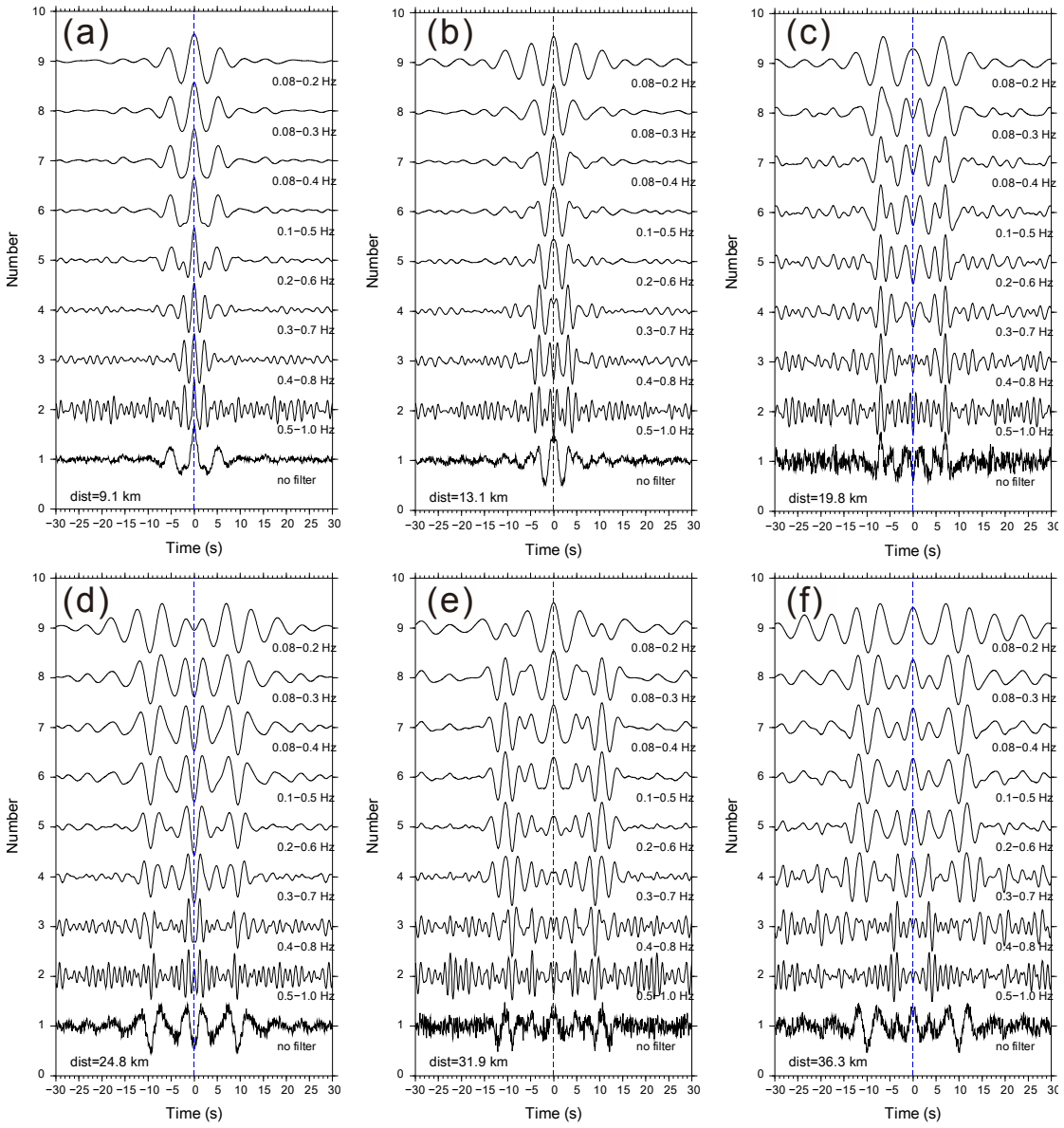

Figure S2. Multiple filter waveforms for station pairs with different interstation distance from 9~36 km. The interstation distance is labeled on the lower-left corner of each subfigure. The parameters of band pass filter is labeled on the lower-right of each waveform.

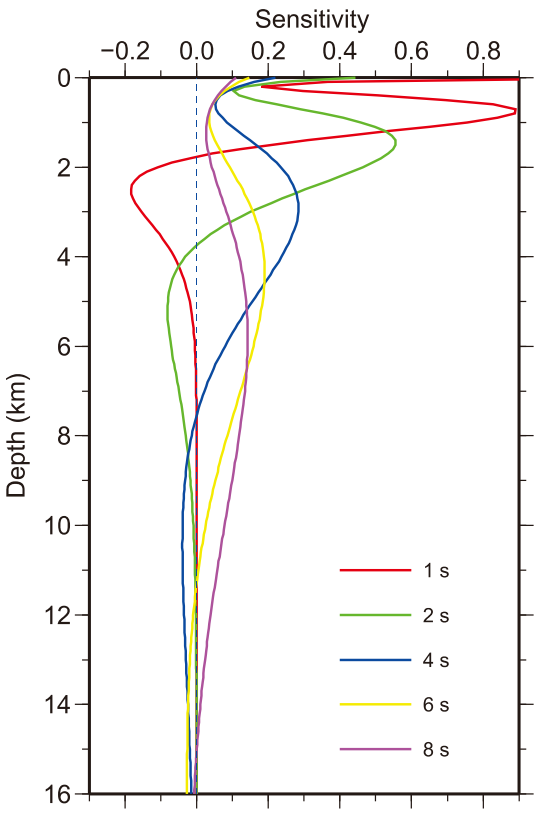

Figure S3. Normalized depth sensitivity kernels for 1~8 s Rayleigh wave group velocity on the S-wave velocity.

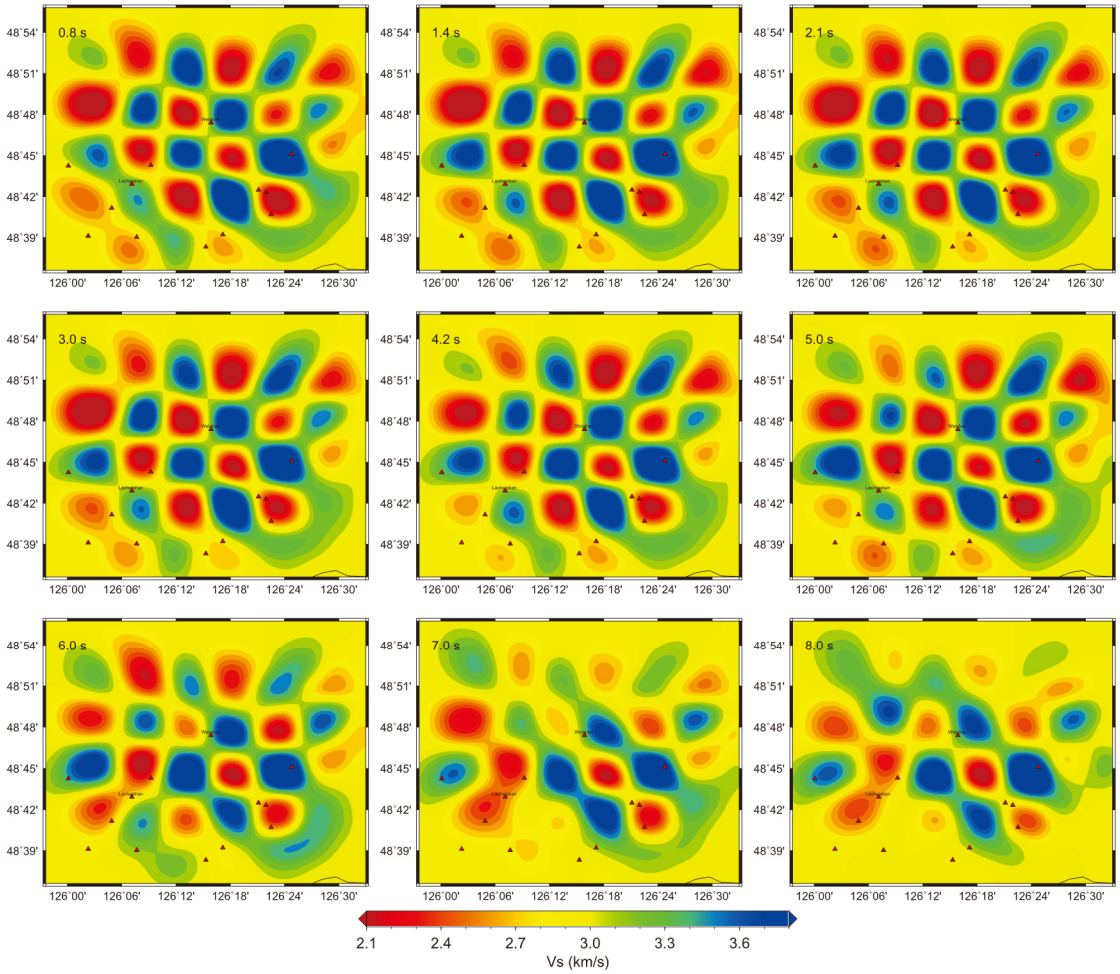

Figure S4. Checkerboard resolution test for different periods of 0.8~8.0 s. The size of each velocity anomaly is 0.07°×0.05°. The red triangles show the locations of volcanoes.

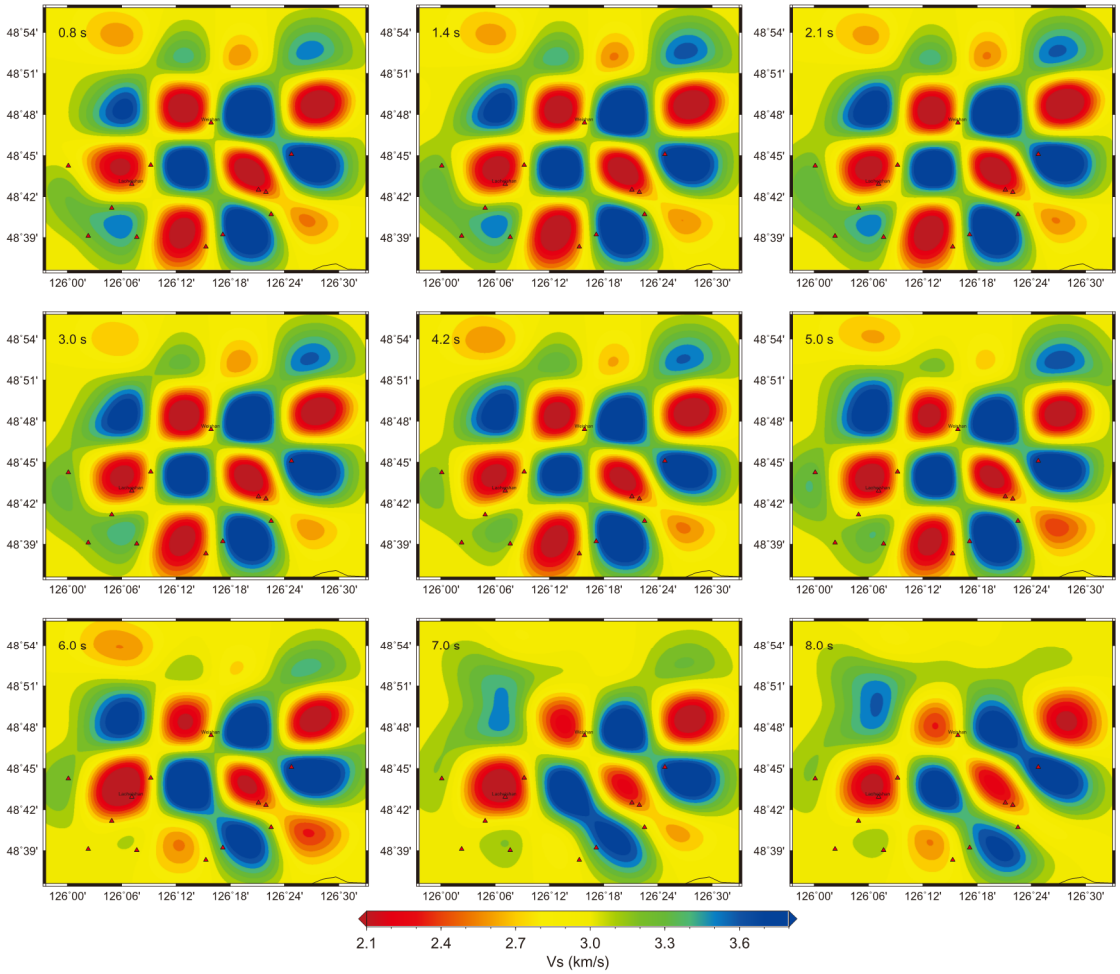

Figure S5. Same figure as Figure S1 but with an anomaly size of 0.11°×0.07°.

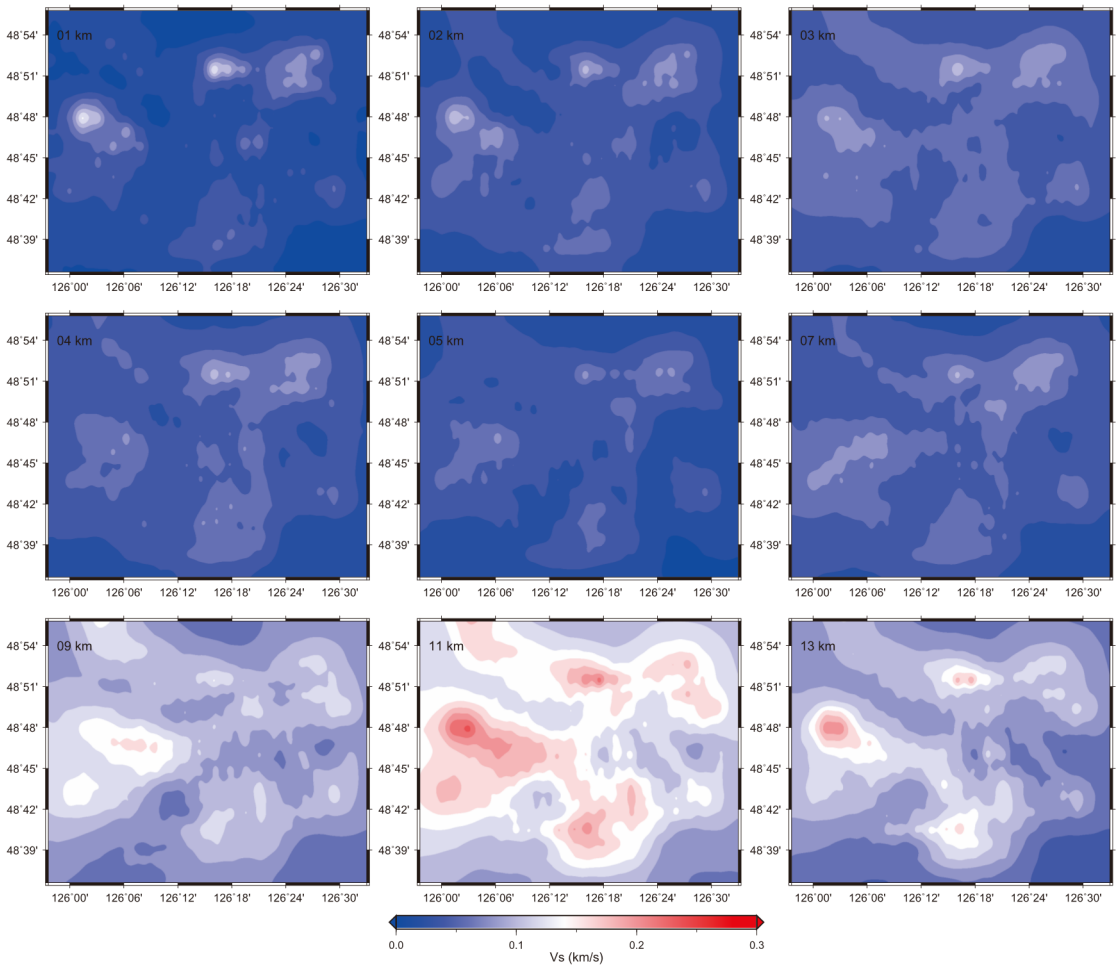

Figure S6. Standard deviation estimation of the shear-wave velocity for each depth, which is computed by the bootstrap method with 200 times random selections of the data set.

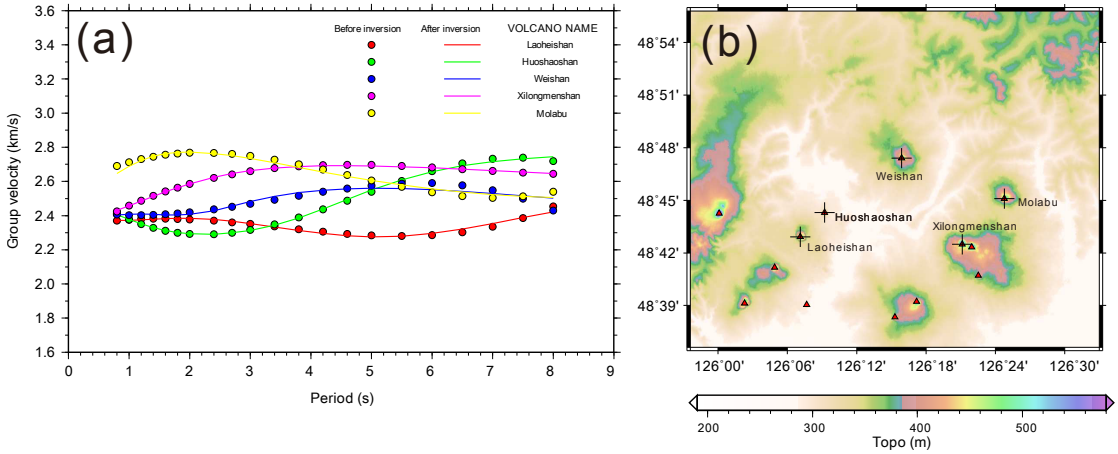

Figure S7. (a) Dispersion curves before and after shear wave velocity inversion. The dispersion are obtained from the location of five volcanos of Laoheishan, Huoshaoshan, Weishan, Xilongmenshan and Molabu, which are shown in figure S7b as black crosses. The results suggest that the dispersion curves from the inverted shear wave velocity models can fit the dispersion curves from the ambient noise tomography very well.